

Token Pruning for In-Context Generation in Diffusion Transformers

Junqing Lin^{1,2} Xingyu Zheng^{2,3} Pei Cheng² Bin Fu² Jingwei Sun¹ Guangzhong Sun¹

Abstract

In-context generation significantly enhances Diffusion Transformers (DiTs) by enabling controllable image-to-image generation through reference examples. However, the resulting input concatenation drastically increases sequence length, creating a substantial computational bottleneck. Existing token reduction techniques, primarily tailored for text-to-image synthesis, fall short in this paradigm as they apply uniform reduction strategies, overlooking the inherent role asymmetry between reference contexts and target latents across spatial, temporal, and functional dimensions. To bridge this gap, we introduce ToPi, a training-free token pruning framework tailored for in-context generation in DiTs. Specifically, ToPi utilizes offline calibration-driven sensitivity analysis to identify pivotal attention layers, serving as a robust proxy for redundancy estimation. Leveraging these layers, we derive a novel influence metric to quantify the contribution of each context token for selective pruning, coupled with a temporal update strategy that adapts to the evolving diffusion trajectory. Empirical evaluations demonstrate that ToPi can achieve over 30% speedup in inference while maintaining structural fidelity and visual consistency across complex image generation tasks.

1. Introduction

Diffusion Transformers (DiTs) (Peebles & Xie, 2023; Xing et al., 2024; Shen et al., 2025) have emerged as the dominant architecture for generative modeling by treating diverse modalities as sequences of latent tokens, effectively capitalizing on the scalability of transformers. Building on this foundation, in-context generation further enhances generation controllability for scenarios such as image-to-image

¹University of Science and Technology of China, Anhui, China

²Tencent PCG, China ³Beihang University, Beijing, China. Correspondence to: Jingwei Sun <sunjw@ustc.edu.cn>, Guangzhong Sun <gzsun@ustc.edu.cn>.

and image-to-video by directly incorporating reference examples into the input sequence without fine-tuning (Liu, 2024; Wan et al., 2025; Kong et al., 2024; Labs et al., 2025; Wu et al., 2025a). However, this paradigm extends the input sequence with reference examples, significantly increasing the computational overhead and memory footprint due to the massive number of tokens. Furthermore, the quadratic complexity of self-attention with respect to sequence length exacerbates this issue, creating a scalability barrier for high-resolution or multi-reference generation tasks.

To mitigate the computational overhead of DiTs, prior works have primarily focused on three strategic directions: accelerating sampling schedules (Lu et al., 2022; Song et al., 2023; Salimans & Ho, 2022; Huang et al., 2025), compressing model parameters (Chen et al., 2024a; Li et al., 2025a; Wang et al., 2025; Zhao et al., 2025), and dynamic computation reduction (Liu et al., 2025b; Zhang et al., 2025a; Bolya et al., 2023). Within the third direction, token reduction methods (Lu et al., 2025; Bolya & Hoffman, 2023; Fang et al., 2025; Kim et al., 2024) are especially attractive: by explicitly limiting the number of active tokens, they directly attack the primary bottleneck induced by long sequences. However, existing token reduction strategies prove ineffective for in-context generation. These methods indiscriminately process reference context and target latents, and overlook that context utility depends on its relevance to the current denoising state. Consequently, existing methods either retain excessive redundancy or blindly prune critical semantic anchors, degrading generation fidelity.

In this paper, we seek a principled answer to a central question in efficient in-context DiTs: when and which tokens can be removed without compromising fidelity? Our starting point is the observation that reference context tokens and target latent tokens play asymmetric roles during denoising. Our systematic analysis reveals that this asymmetry manifests across three interconnected dimensions. (1) Spatially, semantic influence concentrates within a small subset of pivotal layers rather than distributing uniformly. (2) Temporally, redundancy rises as target latents progressively assimilate reference context. (3) Functionally, more complex tasks require denser semantic anchors than simple edits.

Motivated by these findings, we introduce ToPi, a training-free token pruning framework tailored for in-context gener-

ation in DiTs. Specifically, ToPi employs three mechanisms to handle the inherent asymmetry of diffusion tasks. First, it employs a calibration-driven sensitivity analysis to pinpoint pivotal attention layers, serving as a robust proxy for redundancy estimation. Leveraging these layers, we derive a novel influence metric that quantifies the contribution of each reference token, allowing us to selectively discard non-essential context while preserving semantic anchors. Finally, ToPi periodically updates the token selection to synchronize with the evolving diffusion trajectory. Empirical evaluations on Flux.1-Kontext (Labs et al., 2025) and Qwen-Image-Edit (Wu et al., 2025a) demonstrate that ToPi can achieve over 30% speedup in inference on the AnyEdit (Yu et al., 2025) benchmark without compromising structural fidelity or visual consistency.

This paper makes the following contributions:

- We systematically analyze token redundancy during in-context generation in DiTs. We demonstrate that context utility varies across spatial, temporal, and functional dimensions. This characterization highlights the role asymmetry between reference context and target latents, exposing the inadequacy of uniform pruning strategies.
- We introduce ToPi, a training-free framework grounded in signal contribution preservation maximization. We formulate a novel influence metric that identifies importance tokens, coupled with a periodic update strategy to align with the temporal dynamics of diffusion.
- We perform extensive empirical evaluations across diverse image generation benchmarks. The results demonstrate that our approach achieves significant reductions in inference latency without compromising the visual quality or semantic coherence of the output.

2. Related Work

Diffusion Model Acceleration. Research on accelerating Diffusion Probabilistic Models (DPMs) (Ho et al., 2020; Song et al., 2020; Dhariwal & Nichol, 2021) primarily addresses three distinct axes of inefficiency. The first concerns extensive sampling iterations, where advanced solvers (Lu et al., 2022; Song et al., 2020) or distillation techniques (Salimans & Ho, 2022; Song et al., 2023; Huang et al., 2025) compress the inference trajectory. The second targets parameter redundancy, employing quantization (Wu et al., 2024; Chen et al., 2024a; Li et al., 2025a) or pruning (Wang et al., 2025; Zhao et al., 2025) to compact model weights. Our work operates on the third axis: dynamic computation reduction, which optimizes data flow at run-time. It includes temporal strategies (Ma et al., 2024; Zou et al., 2024; Lou et al., 2024; Liu et al., 2025b) that cache or reuse features

across timesteps, as well as spatial strategies that eliminate calculation amount via sparse attention (Zhang et al., 2025c; Yang et al., 2025; Zhang et al., 2025a;b) or through *token reduction* methods (Bolya & Hoffman, 2023; Fang et al., 2025; Kim et al., 2024; Lu et al., 2025) that explicitly reduce sequence length.

Token Reduction: From Discriminative to Generative. Token reduction was initially developed for discriminative Vision Transformers (ViTs) (Rao et al., 2021; Zhai et al., 2022) and Multimodal LLMs (Wu et al., 2023; Caffagni et al., 2024), employing pruning (Rao et al., 2021; Chen et al., 2024b; Zhang et al., 2024; 2025e;d; Zou et al., 2025) or merging (Bolya et al., 2023; Shang et al., 2025; Li et al., 2025b) to alleviate computational overhead. However, applying existing reduction methods to visual in-context generation encounters two structural mismatches. First, there is a *purpose mismatch*: discriminative objectives prioritize high-level semantic abstraction, whereas generative modeling requires dense signal propagation to maintain spatial fidelity. Second, there is a *contextual mismatch* in existing DPM adaptations (Bolya & Hoffman, 2023; Kim et al., 2024; Smith et al., 2024; Wu et al., 2025b; Fang et al., 2025). Most of them are optimized for independent image generation and fail to distinguish the distinct roles of reference context and target latents, neglecting the critical interactions required for in-context generation. ToPi bridges these mismatches by introducing a generative-oriented influence metric to preserve reconstruction features, while simultaneously addressing the redundancy specific to reference tokens to enable efficient context-aware generation.

3. Preliminaries and Motivation

3.1. Preliminaries

We focus on conditional diffusion models operating within the latent space of a pre-trained VAE. The model functions by iteratively denoising noisy tokens $\mathcal{G}^t \in \mathbb{R}^{|\mathcal{G}^t| \times d}$ across timesteps $t = T, \dots, 1$ to recover the clean state \mathcal{G}^0 . Within this framework, in-context generation facilitates image generation conditioned on a fixed sequence of reference tokens $\mathcal{C} \in \mathbb{R}^{|\mathcal{C}| \times d}$ to improve the controllability of the synthesis process. Fundamentally, in-context generation operates by concatenating these reference tokens with the noisy tokens \mathcal{G} along the sequence dimension. This yields a unified input sequence $\mathbf{Z}^t \in \mathbb{R}^{(|\mathcal{G}^t| + |\mathcal{C}|) \times d}$:

$$\mathbf{Z}^t = [\mathcal{G}^t; \mathcal{C}], \quad (1)$$

where $[\cdot; \cdot]$ denotes the concatenation operation. Then, the self-attention mechanism within each DiT block operates globally on this joint sequence. Let \mathbf{H} represent the intermediate features at a given layer; the query, key, and value projections are defined as $\mathbf{Q} = \mathbf{H}\mathbf{W}_Q$, $\mathbf{K} = \mathbf{H}\mathbf{W}_K$, and $\mathbf{V} = \mathbf{H}\mathbf{W}_V$. The resulting attention matrix captures full

bidirectional dependencies:

$$\mathbf{A} = \text{softmax} \left(\frac{\mathbf{Q}\mathbf{K}^\top}{\sqrt{d}} \right). \quad (2)$$

While this unified formulation ensures dense information flow between the target latents and reference contexts, it incurs a computational cost that scales quadratically with the total sequence length.

3.2. Motivation: Redundancy in Contextual Attention

We hypothesize that current architectures suffer from significant inefficiency by failing to account for the role asymmetry between reference context and target latents. Rather than requiring a dense, uniform integration, the generative process relies on sparse, discriminative visual cues. To quantify this, we define the target-aware attention score S_j for a specific reference token $j \in \mathcal{C}$. This metric represents the average attention weight that token j receives from all noisy tokens \mathcal{G} , averaged across heads \mathcal{H} :

$$S_j = \frac{1}{|\mathcal{G}| \cdot |\mathcal{H}|} \sum_{h \in \mathcal{H}} \sum_{i \in \mathcal{G}} A_{ij,h}. \quad (3)$$

Our empirical analysis confirms that token importance is highly non-uniform, characterized by three dimensions of asymmetry: spatial concentration, temporal evolution, and functional anchoring.

Spatial: Concentration in Pivotal Layers. Fig. 1 reveals spatial asymmetry in attention distribution across network layers. Rather than exhibiting uniform semantic diffusion, attention mass concentrates heavily within a sparse subset of pivotal layers while the remaining layers contribute negligible weight. Meanwhile, this stratification is input-invariant, indicating that context retrieval is a layer-specialized process rather than a global property. Consequently, these pivotal layers function as sufficient proxies for global token importance, enabling reliable redundancy estimation without requiring full-layer evaluation.

Temporal: Evolution over Timesteps. Contextual interaction exhibits two temporal dynamics. (1) *Fluctuating*

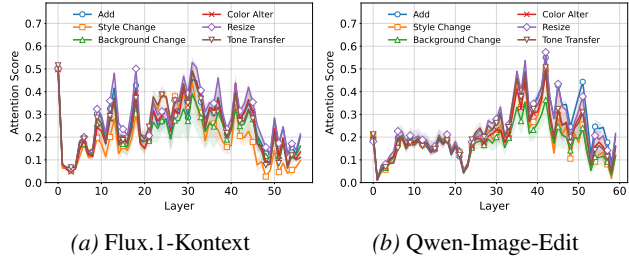


Figure 1. Layer-wise distribution of the total target-aware attention score ($\sum S_j$), averaged across timesteps.

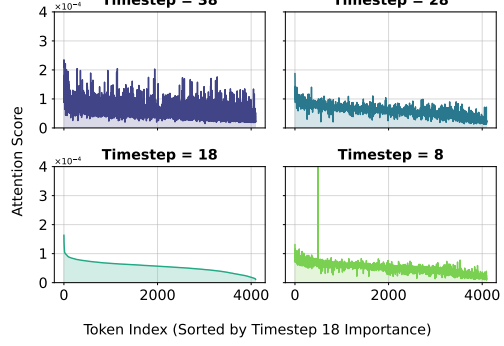


Figure 2. Evolution of individual target-aware attention scores (S_j) for reference tokens across timesteps, averaged across layers.

Token Relevance. Fig. 2 reveals that the relative importance of individual tokens shifts dynamically throughout the generation process. Consequently, strategies relying on a fixed set of selected tokens during the entire denoising process are inherently suboptimal. (2) *Global Attentional Decay*. As shown in Fig. 3, the total score follows a trajectory of temporal decay. Early high-noise stages rely heavily on reference features for structural guidance, whereas later stages transition toward self-contained refinement.

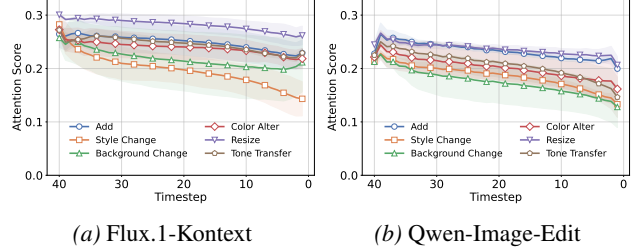


Figure 3. Temporal trajectory of the total attention score ($\sum S_j$) under different task conditions, averaged across layers.

Functional: Task-Dependent Anchoring. Quantitatively, Fig. 3 reveals that total reference attention remains consistently low (< 0.3), indicating that the generation process is predominantly driven by self-attention within the noisy tokens. This data characterizes reference tokens functioning primarily as auxiliary semantic anchors rather than dense constructive elements. Crucially, the reliance on these anchors is dictated by functional asymmetry: high-fidelity tasks (e.g., Resize) sustain elevated attention levels to preserve structural details, whereas loose-constraint tasks (e.g., Style Change) exhibit a rapid decline in attention mass. This task-dependent variability mandates that computational allocation be dynamically modulated to match the specific functional demands of the intervention.

4. Method

As analyzed in Sec. 3.2, the reference context acts as a supportive resource, from which target latents selectively

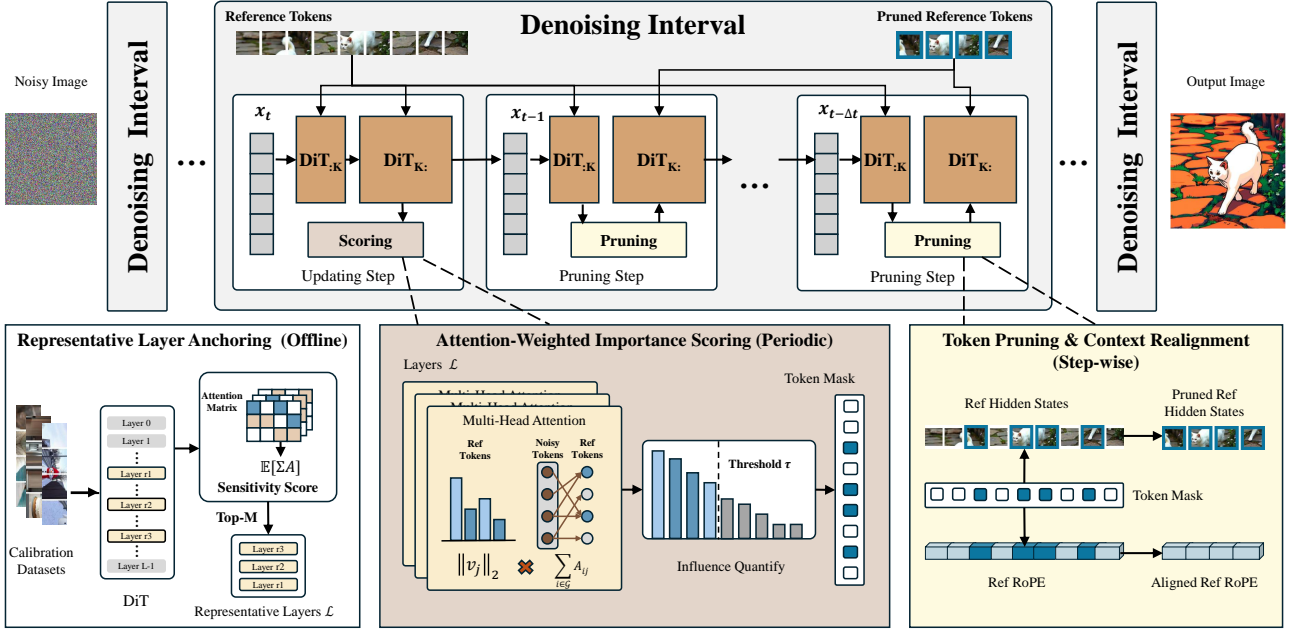


Figure 4. Overview of ToPi. The upper panel depicts the denoising trajectory, which contains multiple denoising intervals. Each interval comprises a mask updating step and multiple token pruning steps. This process is controlled by three stratified mechanisms detailed in the lower panels: (1) **Offline Calibration**: One-time identification of representative layers \mathcal{L} of a DiT to filter out insensitive layers. (2) **Periodic Scoring**: Importance scoring and mask updates every ΔT steps to adapt to semantic shifts. (3) **Step-wise Pruning**: Instant token pruning and context realignment applied at each denoising step.

attend to only sparse semantic regions. To leverage this inherent redundancy, we introduce **ToPi**, a training-free and dynamic token pruning framework tailored for in-context generation in DiTs. Rather than processing the full sequence, ToPi dynamically extracts a minimal sufficient subset \mathcal{C}' from the reference tokens \mathcal{C} , retaining only the semantic core essential for high-fidelity generation.

As illustrated in Fig. 4, ToPi employs three mechanisms sequentially. (1) **Representative Layer Anchoring** identifies semantically dense layers offline; (2) **Attention-Weighted Importance Scoring** periodically computes token importance scores and updates the retention mask during inference; and (3) **Token Pruning & Context Realignment** applies the mask at each timestep, directly accelerating the generative process. The complete algorithmic formulation is provided in Appendix B.

4.1. Representative Layer Anchoring

Modern diffusion architectures typically consist of numerous attention layers. Using all layers to estimate importance imposes two primary constraints. First, aggregating attention statistics across the entire network introduces substantial overhead, which can negate the efficiency gains from pruning. Second, empirical analysis reveals that layers exhibit significant heterogeneity in their sensitivity to the context \mathcal{C} . The inclusion of layers with negligible sensitivity

introduces noise, thereby compromising the fidelity of token importance rankings. To mitigate these limitations, we isolate a subset of *Representative Layers*. These layers encapsulate the dominant interactions with the visual context and serve as a robust proxy for the global context processing of the full model.

Guided by our observation in Sec. 3.2, which demonstrates that the spatial location of pivotal layers remains consistent across diverse tasks, we constructed \mathcal{D}_{calib} to be a stratified subset covering multiple categories. Consider the ℓ -th attention layer, which incorporates a set of attention heads \mathcal{H} . We denote the query features (noisy tokens) as $\mathbf{Q}^{(\ell)} \in \mathbb{R}^{|\mathcal{H}| \times |\mathcal{G}| \times d}$ and the key features (reference tokens) as $\mathbf{K}^{(\ell)} \in \mathbb{R}^{|\mathcal{H}| \times |\mathcal{C}| \times d}$. The normalized attention weights are given by $\mathbf{A}^{(\ell)} = \text{Softmax}(\frac{\mathbf{Q}^{(\ell)}(\mathbf{K}^{(\ell)})^\top}{\sqrt{d}})$. We define the *Context Sensitivity Score* $S^{(\ell)}$ as the expected attention mass accumulated across the calibration set:

$$S^{(\ell)} = \mathbb{E}_{\mathbf{x} \sim \mathcal{D}_{calib}} \left[\sum_{h \in \mathcal{H}} \sum_{i \in \mathcal{G}} \sum_{j \in \mathcal{C}} A_{hij}^{(\ell)} \right]. \quad (4)$$

A higher value of $S^{(\ell)}$ indicates that the layer exhibits a stronger dependency on the provided context \mathcal{C} , distinguishing it as a Representative Layer. We isolate the Top- M layers with the highest sensitivity scores to construct the

representative set \mathcal{L} :

$$\mathcal{L} = \text{Top-M}_{\ell \in \{0, \dots, L-1\}} \left\{ S^{(\ell)} \right\}. \quad (5)$$

4.2. Attention-Weighted Importance Scoring

Theoretical Objective. To preserve contextual semantic integrity, we formulate the pruning objective as a signal contribution preservation problem. Specifically, we consider the attention output \mathbf{y}_i for the i -th token as a linear combination of value vectors from the entire input sequence $\mathcal{G} \cup \mathcal{C}$:

$$\mathbf{y}_i = \sum_{k \in \mathcal{G} \cup \mathcal{C}} A_{ik} \mathbf{v}_k. \quad (6)$$

By decomposing this output into individual signal components, the specific contribution of the k -th token to the i -th output is captured by the vector \mathbf{c}_{ik} :

$$\mathbf{c}_{ik} := A_{ik} \mathbf{v}_k. \quad (7)$$

In this formulation, token importance is quantified by the magnitude of its contribution to the final representation, effectively integrating attention weights with feature strength. This metric ensures that a token with moderate attention weights can still exert significant influence if it possesses a large feature vector. To minimize cumulative information loss across the target latents, we seek to identify the token k yielding the minimal aggregate signal norm:

$$\min_k \sum_{i \in \mathcal{G}} \|\mathbf{c}_{ik}\|_2 = \min_k \sum_{i \in \mathcal{G}} A_{ik} \|\mathbf{v}_k\|_2. \quad (8)$$

Metric Formulation. Building upon this theoretical insight, we generalize this criterion to the full Transformer architecture. Given that signal contributions are additive across independent subspaces, we assess a token’s global importance by aggregating its contributions. Accordingly, we define the **Token Influence Score** I_j as the sum of weighted norms across all attention heads \mathcal{H} and layers \mathcal{L} :

Definition 4.1 (Token Influence Score). For a context token j , its influence I_j is the cumulative signal magnitude weighted by its global attention reception:

$$I_j = \sum_{\ell \in \mathcal{L}} \sum_{h \in \mathcal{H}} \|\mathbf{v}_{j,h}^\ell\|_2 \cdot \sum_{i \in \mathcal{G}} A_{i,j,h}^\ell. \quad (9)$$

4.3. Token Pruning & Context Realignment

Fidelity-Constrained Pruning. Given the importance metric I_j , a fixed pruning ratio is suboptimal because the information density of the reference context varies across tasks. We therefore formulate token pruning as a cardinality minimization problem subject to a fidelity constraint. It seeks the minimal subset of context tokens $\mathcal{C}' \subset \mathcal{C}$ that

preserves at least a fraction τ of the total information mass $I_{\text{total}} = \sum_{j \in \mathcal{C}} I_j$:

$$\min_{\mathcal{C}' \subset \mathcal{C}} |\mathcal{C}'| \quad \text{s.t.} \quad \sum_{j \in \mathcal{C}'} I_j \geq \tau \cdot I_{\text{total}}, \quad (10)$$

where the hyperparameter $\tau \in [0, 1]$ controls the fidelity-efficiency trade-off. This adaptive formulation automatically modulates the computational budget based on the semantic complexity of the task. Since the computational cost of each token is uniform, the optimal solution to Eq. (10) is obtained via greedy accumulation. Specifically, we sort the context tokens by their influence scores such that $I_{\pi(1)} \geq I_{\pi(2)} \geq \dots \geq I_{\pi(N)}$ and select the Top- K tokens, where K is the smallest integer satisfying $\sum_{m=1}^K I_{\pi(m)} \geq \tau \cdot I_{\text{total}}$.

Temporal Adaptation. As noted in Sec. 3.2, the semantic focus of diffusion models evolves along the denoising trajectory. To balance adaptation precision and inference efficiency, ToPi adopts a piecewise-constant approximation for context selection. Instead of recomputing token importance at every step, we define a sparse set of anchor timesteps $\mathcal{T}_{\text{anchor}} \subset \{T, \dots, 0\}$ (e.g., evenly spaced with a fixed stride). At anchor points, we utilize the full context to update the active context set \mathcal{C}'_t for subsequent steps. Formally, the context for the timestep t is determined by:

$$\mathcal{C}'_t = \begin{cases} \text{Solve Eq. (10),} & \text{if } t \in \mathcal{T}_{\text{anchor}} \\ \mathcal{C}'_{t+1}, & \text{otherwise} \end{cases} \quad (11)$$

This design preserves the overall trend of semantic evolution in the context (e.g., from coarse structure to fine textures), while amortizing the cost of scoring and selection across multiple steps.

Context Realignment. Based on the informative subset \mathcal{C}'_t , we employ a hard selection strategy to compress the reference context. Note that the initial K layers are exempted to preserve essential low-level feature extraction. Furthermore, addressing the positional sensitivity of Rotary Positional Embeddings (RoPE) necessitates a synchronized gather operation on both the hidden states \mathbf{H} and their corresponding position indices \mathbf{P} :

$$\hat{\mathbf{H}} = \mathbf{H}[\mathcal{C}'_t], \quad \hat{\mathbf{P}} = \mathbf{P}[\mathcal{C}'_t]. \quad (12)$$

This aligned indexing mechanism ensures that the original spatial semantics and relative geometric relationships among retained tokens are preserved for subsequent layers.

4.4. Computational Overhead Analysis

The overhead introduced by our framework decomposes into two components with different temporal frequencies:

- **Periodic Mask Update:** This phase includes Importance Scoring and Subset Selection, with complexities

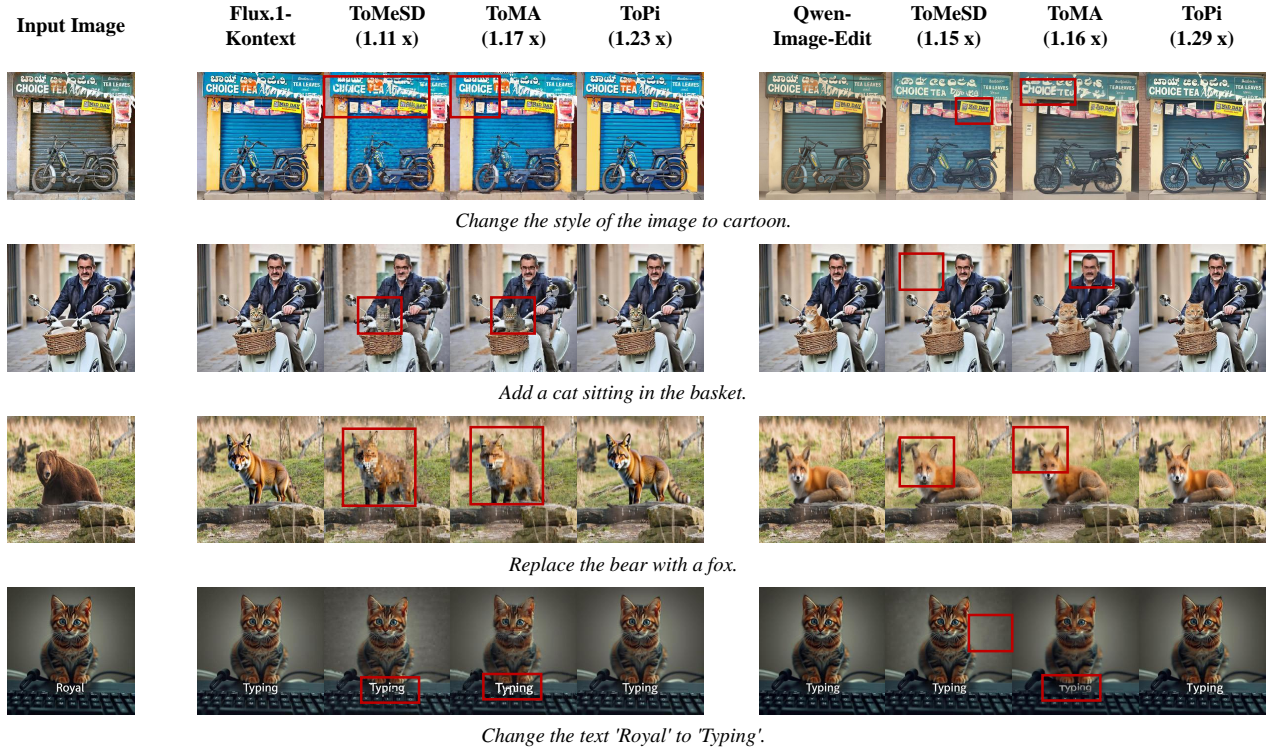


Figure 5. Qualitative comparison on the AnyEdit benchmark. We compare Flux.1-Kontext (left) against Qwen-Image-Edit (right). Best viewed zoomed in. Additional quantitative analyses are provided in Appendix D.

of $O(|\mathcal{L}| \cdot |\mathcal{G}| \cdot |\mathcal{C}|)$ and $O(|\mathcal{C}| \log |\mathcal{C}|)$, respectively. Executed once per update interval, these costs are amortized over ΔT steps, ensuring the effective per-step overhead remains negligible.

- **Per-Step Pruning and Realignment:** At each diffusion timestep, we apply a global pruning operation. This reduces the instantaneous overhead to a single linear gather operation with a complexity of $O(|\mathcal{C}'|)$.

A comprehensive derivation of FLOPs and runtime benchmarks is provided in Appendix F.

5. Experiments

5.1. Experimental Setup

Models and Tasks. We integrate ToPi into Flux.1-Kontext (Labs et al., 2025) and Qwen-Image-Edit (Wu et al., 2025a) to demonstrate versatility. Evaluations are conducted on the AnyEdit (Yu et al., 2025) benchmark across four sub-tasks: (a) Camera Move Editing, (b) Global Editing, (c) Implicit Editing and (d) Local Editing.

Baselines. We benchmark ToPi against ToMeSD (Bolya & Hoffman, 2023) and ToMA (Lu et al., 2025). To provide a comprehensive evaluation, we report results for two configurations:

(1) **Standard**, where pruning operates globally on the entire sequence $(\mathcal{G} \cup \mathcal{C})$; and (2) **Reference-Only** (denoted with *), where we explicitly mask the noisy tokens \mathcal{G} to force baselines to prune only reference tokens \mathcal{C} .

Evaluation Metrics. To quantitatively assess generation quality, we report three standard metrics: Peak Signal-to-Noise Ratio (PSNR) for pixel-level fidelity, Structural Similarity Index (SSIM) (Wang et al., 2004) for structural consistency (including luminance and contrast), and Learned Perceptual Image Patch Similarity (LPIPS) (Zhang et al., 2018) for perceptual similarity aligned with human vision. In our experiments, images generated via full-context inference serve as the ground truth. Higher PSNR and SSIM, and lower LPIPS, indicate superior performance.

Implementation Details. Unless otherwise specified, we set the pruning threshold to $\tau = 0.85$. To balance temporal adaptability with computational overhead, the pruning mask is updated at an interval of $\Delta T = 10$. Furthermore, we exempt the initial 10 layers from this pruning process.

5.2. Main Results

To evaluate the efficacy of ToPi, we conduct a comprehensive benchmarking analysis encompassing both qualitative

Table 1. Quantitative comparison across different categories. We highlight the best results in **bold** and mark our method with a gray background. Speedup values denote the acceleration relative to the full-context inference latency. Experiments are conducted on NVIDIA A100 GPUs for Flux.1-Kontext and NVIDIA H20 GPUs for Qwen-Image-Edit, using fixed random seeds to ensure reproducibility.

Category	Method	Flux.1-Kontext				Qwen-Image-Edit			
		PSNR↑	SSIM↑	LPIPS↓	Speed↑	PSNR↑	SSIM↑	LPIPS↓	Speed↑
Camera Move	ToMeSD	20.87	0.678	0.231	1.05	23.18	0.737	0.191	1.14
	ToMeSD*	21.24	0.685	0.220	1.10	22.58	0.724	0.186	1.17
	ToMA	21.79	0.702	0.213	1.17	21.33	0.717	0.221	1.16
	ToMA*	21.99	0.695	0.231	1.18	21.32	0.717	0.214	1.16
	Ours	25.01	0.762	0.156	1.24	25.07	0.812	0.117	1.31
Global Edit	ToMeSD	18.24	0.589	0.327	1.13	18.72	0.613	0.283	1.14
	ToMeSD*	17.66	0.574	0.349	1.18	19.03	0.621	0.256	1.17
	ToMA	19.79	0.625	0.307	1.17	18.95	0.623	0.280	1.16
	ToMA*	18.68	0.591	0.333	1.18	18.83	0.622	0.274	1.16
	Ours	22.46	0.719	0.207	1.26	21.04	0.690	0.189	1.33
Implicit Change	ToMeSD	23.33	0.788	0.178	1.13	25.56	0.801	0.135	1.16
	ToMeSD*	23.06	0.772	0.189	1.16	25.66	0.799	0.124	1.19
	ToMA	24.37	0.793	0.179	1.18	21.75	0.774	0.176	1.17
	ToMA*	24.39	0.787	0.187	1.18	21.71	0.774	0.169	1.17
	Ours	29.40	0.881	0.085	1.21	28.05	0.848	0.085	1.27
Local Edit	ToMeSD	21.36	0.743	0.203	1.13	23.33	0.763	0.158	1.15
	ToMeSD*	21.65	0.748	0.193	1.17	22.90	0.753	0.153	1.18
	ToMA	22.69	0.772	0.178	1.17	21.48	0.738	0.185	1.16
	ToMA*	22.43	0.756	0.195	1.18	21.46	0.738	0.177	1.16
	Ours	27.55	0.868	0.087	1.21	25.82	0.823	0.103	1.27

visual fidelity and quantitative performance metrics.

5.2.1. QUALITATIVE RESULTS

Existing token reduction methods (e.g., ToMeSD and ToMA) often compromise generation fidelity, manifesting as perceptual blurring artifacts or semantic drift from the reference. As visually corroborated in Fig. 5, these baseline methods struggle to retain fine-grained textures under high compression regimes, leading to structural deterioration. Representative instances of this degradation include the illegible text in the garage scene (Row 1) and the over-smoothed fur texture in the animal replacement task (Row 3). Conversely, ToPi demonstrates superior perceptual fidelity. It effectively preserves critical high-frequency details and produces outputs that remain visually close to the computationally intensive full-context baseline.

5.2.2. QUANTITATIVE RESULTS

Tab. 1 reports the quantitative evaluation on Flux.1-Kontext and Qwen-Image-Edit models. Our framework consistently achieves state-of-the-art performance, outperforming baselines by substantial margins across all metrics and tasks. Specifically, in tasks demanding high structural fidelity such as *Implicit Change*, our method yields a remarkable gain of over 5 in PSNR compared to ToMA (29.40 vs. 24.37 on Flux.1-Kontext). Similarly, in the *Local Editing* scenario,

we minimize the LPIPS to 0.087, effectively halving the error relative to the best-performing baseline (0.178).

Importantly, these quality gains do not come at the cost of latency. As detailed in Tab. 1, our approach consistently establishes a superior quality–latency Pareto frontier. Unlike baselines that compromise visual quality for moderate acceleration ($1.05\times$ – $1.18\times$), our method achieves the highest inference throughput, reaching speedups of up to $1.33\times$ on Qwen-Image-Edit. This efficiency stems from our lightweight pruning paradigm, which effectively eliminates redundancy in reference tokens with negligible run-time computational overhead.

Notably, we also compare against “Reference-Only” baseline variants (marked with *), where pruning is manually constrained to reference tokens \mathcal{C} to favor preservation. Even with this adaptation, our method consistently outperforms them (e.g., 25.01 vs. 21.24 in *Camera Move*), proving that our dedicated selection mechanism is far more effective than simply masking existing pruning algorithms.

5.3. Orthogonality with Temporal Acceleration

To verify the orthogonality with temporal acceleration techniques, we deployed ToPi alongside TeaCache (Liu et al., 2025a). Empirical results show that the combination achieves a cumulative speedup of $2.34\times$. Qualitatively, as shown in Fig. 6, ToPi complements the temporal accel-

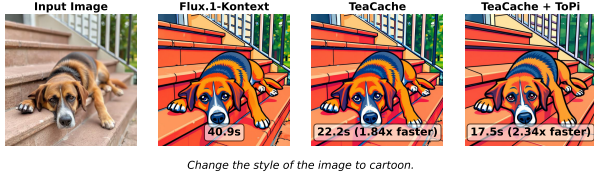


Figure 6. Qualitative demonstration of the orthogonality between ToPi and TeaCache. ToPi preserves high-precision semantic details even when combined with TeaCache.

eration of TeaCache by acting as a high-precision spatial filter that preserves semantic details even when features are reused across timesteps, offering a superior trade-off compared to using either method alone.

5.4. Ablation Study

In this section, we conduct comprehensive ablation studies to validate the effectiveness of key components in ToPi. To ensure a consistent and rigorous evaluation, we utilize the Flux.1-Kontext model as our primary testbed and standardize the token pruning ratio at 50% (implemented via a static Top-K selection) across all experiments. This strict constraint serves as a stress test, allowing us to isolate the contribution of each design choice, specifically the layer selection strategy and the importance metric definition, independent of the adaptive mechanism. Additionally, Appendix E provides further analyses, including the impact of temporal adaptation, a comparison between token reduction strategies, and the effect of the pruning threshold τ .

Table 2. Ablation study on Layer Selection Strategies.

Category	Method	PSNR \uparrow	SSIM \uparrow	LPIPS \downarrow
Camera Move	Random	26.80	0.819	0.112
	All	27.43	0.822	0.113
	Ours	27.69	0.828	0.108
Global Editing	Random	23.13	0.740	0.184
	All	23.64	0.751	0.176
	Ours	23.76	0.754	0.173
Implicit Change	Random	29.31	0.868	0.090
	All	30.00	0.870	0.091
	Ours	30.02	0.874	0.088
Local Editing	Random	26.62	0.849	0.099
	All	27.48	0.854	0.097
	Ours	27.52	0.862	0.091

Layer Selection Strategy. To evaluate the layer selection method proposed in Sec. 4.1, we compare our context sensitivity score $S^{(\ell)}$ with two baselines: (1) *Random*, which uniformly samples 3 layers; and (2) *All*, which aggregates scores from all layers. As shown in Tab. 2, our strategy performs matches or slightly exceeds the *All* baseline. This indicates that using every layer introduces noise from irrelevant layers, which weakens the important semantic signals.

By selecting the layers with the highest $S^{(\ell)}$, our method ensures that token importance is derived only from the most useful interactions, allowing us to achieve robust results using a smaller subset of layers.

Table 3. Ablation study on Token Pruning Metrics.

Category	Method	PSNR \uparrow	SSIM \uparrow	LPIPS \downarrow
Camera Move	Similarity	17.21	0.657	0.292
	Attn-Only	27.39	0.825	0.111
	Ours	27.69	0.828	0.108
Global Editing	Similarity	17.06	0.629	0.312
	Attn-Only	23.60	0.751	0.173
	Ours	23.76	0.754	0.173
Implicit Change	Similarity	17.64	0.754	0.265
	Attn-Only	29.41	0.867	0.092
	Ours	30.02	0.874	0.088
Local Editing	Similarity	17.32	0.720	0.251
	Attn-Only	27.03	0.856	0.095
	Ours	27.52	0.862	0.091

Pruning Metric. We evaluate the *Token Influence Score* (Eq. 9) against two baselines: (1) *Feature Similarity*, ranking tokens by cosine similarity; and (2) *Attn-Only*, relying solely on the attention map \mathbf{A} . Tab. 3 shows that *Feature Similarity* degrades performance, indicating semantic alignment is a poor proxy for functional importance. While *Attn-Only* is competitive, our method achieves superior fidelity by incorporating the value magnitude $\|\mathbf{V}\|$. This confirms that attention weights alone are insufficient; influential tokens must possess both high attention and significant magnitude. By integrating $\|\mathbf{V}\|$, we remove spurious high-attention tokens to capture the most critical feature updates.

6. Conclusion

In this paper, we introduce ToPi, a novel training-free framework designed to accelerate in-context generation within Diffusion Transformers. Through a systematic analysis of spatiotemporal attention dynamics, we identify that the processing of contextual reference tokens is characterized by significant redundancy. Departing from prior heuristic-based pruning, ToPi employs an influence-aware metric derived directly from singular contribution preservation. This formulation enables the precise identification and pruning of low-utility tokens while maintaining the semantic fidelity of the generation process. Extensive evaluations across diverse architectures demonstrate that ToPi establishes a superior trade-off between inference latency and generation quality, delivering speedups with negligible perceptual degradation. By demonstrating that sparse token retention is sufficient for robust in-context generation, this work facilitates efficient model deployment and highlights a promising direction for future input-adaptive generative models.

Impact Statement

This paper presents work whose goal is to advance the field of Machine Learning. There are many potential societal consequences of our work, none which we feel must be specifically highlighted here.

References

Bolya, D. and Hoffman, J. Token merging for fast stable diffusion. *CVPR Workshop on Efficient Deep Learning for Computer Vision*, 2023.

Bolya, D., Fu, C.-Y., Dai, X., Zhang, P., Feichtenhofer, C., and Hoffman, J. Token merging: Your ViT but faster. In *International Conference on Learning Representations*, 2023.

Caffagni, D., Cocchi, F., Barsellotti, L., Moratelli, N., Sarto, S., Baraldi, L., Cornia, M., and Cucchiara, R. The revolution of multimodal large language models: a survey. *arXiv preprint arXiv:2402.12451*, 2024.

Chen, L., Meng, Y., Tang, C., Ma, X., Jiang, J., Wang, X., Wang, Z., and Zhu, W. Q-dit: Accurate post-training quantization for diffusion transformers, 2024a.

Chen, L., Zhao, H., Liu, T., Bai, S., Lin, J., Zhou, C., and Chang, B. An image is worth 1/2 tokens after layer 2: Plug-and-play inference acceleration for large vision-language models. In *European Conference on Computer Vision*, pp. 19–35, 2024b.

Dhariwal, P. and Nichol, A. Diffusion models beat gans on image synthesis. *Advances in neural information processing systems*, 34:8780–8794, 2021.

Fang, H., Tang, S., Cao, J., Zhang, E., Tang, F., and Lee, T.-Y. Attend to not attended: Structure-then-detail token merging for post-training dit acceleration. In *Proceedings of the Computer Vision and Pattern Recognition Conference*, pp. 18083–18092, 2025.

Ho, J., Jain, A., and Abbeel, P. Denoising diffusion probabilistic models. *Advances in neural information processing systems*, 33:6840–6851, 2020.

Huang, X., Li, Z., He, G., Zhou, M., and Shechtman, E. Self forcing: Bridging the train-test gap in autoregressive video diffusion. *arXiv preprint arXiv:2506.08009*, 2025.

Kim, M., Gao, S., Hsu, Y.-C., Shen, Y., and Jin, H. Token fusion: Bridging the gap between token pruning and token merging. In *Proceedings of the IEEE/CVF Winter Conference on Applications of Computer Vision*, pp. 1383–1392, 2024.

Kong, W., Tian, Q., Zhang, Z., Min, R., Dai, Z., Zhou, J., Xiong, J., Li, X., Wu, B., Zhang, J., et al. Hunyuan-video: A systematic framework for large video generative models. *arXiv preprint arXiv:2412.03603*, 2024.

Labs, B. F., Batifol, S., Blattmann, A., Boesel, F., Consul, S., Diagne, C., Dockhorn, T., English, J., English, Z., Esser, P., Kulal, S., Lacey, K., Levi, Y., Li, C., Lorenz, D., Müller, J., Podell, D., Rombach, R., Saini, H., Sauer, A., and Smith, L. Flux.1 kontext: Flow matching for in-context image generation and editing in latent space, 2025. URL <https://arxiv.org/abs/2506.15742>.

Li, M., Lin, Y., Zhang, Z., Cai, T., Li, X., Guo, J., Xie, E., Meng, C., Zhu, J.-Y., and Han, S. Svdquant: Absorbing outliers by low-rank components for 4-bit diffusion models. In *The Thirteenth International Conference on Learning Representations*, 2025a.

Li, S., Zhang, L., Wang, Z., Tian, J., Tan, C., Liu, Z., Yu, C., Xie, Q., Lu, H., Wang, H., et al. Mergevq: A unified framework for visual generation and representation with disentangled token merging and quantization. In *Proceedings of the Computer Vision and Pattern Recognition Conference*, pp. 19713–19723, 2025b.

Liu, F., Zhang, S., Wang, X., Wei, Y., Qiu, H., Zhao, Y., Zhang, Y., Ye, Q., and Wan, F. Timestep embedding tells: It's time to cache for video diffusion model. In *Proceedings of the Computer Vision and Pattern Recognition Conference*, pp. 7353–7363, 2025a.

Liu, J., Zou, C., Lyu, Y., Chen, J., and Zhang, L. From reusing to forecasting: Accelerating diffusion models with taylorseers. *arXiv preprint arXiv:2503.06923*, 2025b.

Liu, S. Zero-shot voice conversion with diffusion transformers. *arXiv preprint arXiv:2411.09943*, 2024.

Lou, J., Luo, W., Liu, Y., Li, B., Ding, X., Hu, W., Cao, J., Li, Y., and Ma, C. Token caching for diffusion transformer acceleration. *arXiv preprint arXiv:2409.18523*, 2024.

Lu, C., Zhou, Y., Bao, F., Chen, J., Li, C., and Zhu, J. Dpm-solver: A fast ode solver for diffusion probabilistic model sampling in around 10 steps. *Advances in neural information processing systems*, 35:5775–5787, 2022.

Lu, W., Zheng, S., Xia, Y., and Wang, S. ToMA: Token merge with attention for diffusion models. In *Forty-second International Conference on Machine Learning*, 2025. URL <https://openreview.net/forum?id=5118tvuIxo>.

Ma, X., Fang, G., and Wang, X. Deepcache: Accelerating diffusion models for free. In *The IEEE/CVF Conference on Computer Vision and Pattern Recognition*, 2024.

Peebles, W. and Xie, S. Scalable diffusion models with transformers. In *Proceedings of the IEEE/CVF international conference on computer vision*, pp. 4195–4205, 2023.

Rao, Y., Zhao, W., Liu, B., Lu, J., Zhou, J., and Hsieh, C.-J. Dynamicvit: Efficient vision transformers with dynamic token sparsification. *Advances in neural information processing systems*, 34:13937–13949, 2021.

Salimans, T. and Ho, J. Progressive distillation for fast sampling of diffusion models. *arXiv preprint arXiv:2202.00512*, 2022.

Shang, Y., Cai, M., Xu, B., Lee, Y. J., and Yan, Y. Llava-prumerge: Adaptive token reduction for efficient large multimodal models. In *Proceedings of the IEEE/CVF International Conference on Computer Vision*, pp. 22857–22867, 2025.

Shen, H., Zhang, J., Xiong, B., Hu, R., Chen, S., Wan, Z., Wang, X., Zhang, Y., Gong, Z., Bao, G., et al. Efficient diffusion models: A survey. *arXiv preprint arXiv:2502.06805*, 2025.

Smith, E., Saxena, N., and Saha, A. Todo: token downsampling for efficient generation of high-resolution images. In *Proceedings of the Thirty-Third International Joint Conference on Artificial Intelligence*, pp. 8801–8804, 2024.

Song, J., Meng, C., and Ermon, S. Denoising diffusion implicit models. In *International Conference on Learning Representations*, 2020.

Song, Y., Dhariwal, P., Chen, M., and Sutskever, I. Consistency models. In *Proceedings of the 40th International Conference on Machine Learning*, pp. 32211–32252, 2023.

Wan, T., Wang, A., Ai, B., Wen, B., Mao, C., Xie, C.-W., Chen, D., Yu, F., Zhao, H., Yang, J., Zeng, J., Wang, J., Zhang, J., Zhou, J., Wang, J., Chen, J., Zhu, K., Zhao, K., Yan, K., Huang, L., Feng, M., Zhang, N., Li, P., Wu, P., Chu, R., Feng, R., Zhang, S., Sun, S., Fang, T., Wang, T., Gui, T., Weng, T., Shen, T., Lin, W., Wang, W., Wang, W., Zhou, W., Wang, W., Shen, W., Yu, W., Shi, X., Huang, X., Xu, X., Kou, Y., Lv, Y., Li, Y., Liu, Y., Wang, Y., Zhang, Y., Huang, Y., Li, Y., Wu, Y., Liu, Y., Pan, Y., Zheng, Y., Hong, Y., Shi, Y., Feng, Y., Jiang, Z., Han, Z., Wu, Z.-F., and Liu, Z. Wan: Open and advanced large-scale video generative models. *arXiv preprint arXiv:2503.20314*, 2025.

Wang, K., Chen, J., Li, H., Mi, Z., and Zhu, J. Sparsedm: Toward sparse efficient diffusion models. In *IEEE International Conference on Multimedia and Expo.*, 2025.

Wang, Z., Bovik, A. C., Sheikh, H. R., and Simoncelli, E. P. Image quality assessment: from error visibility to structural similarity. *IEEE transactions on image processing*, 13(4):600–612, 2004.

Wu, C., Li, J., Zhou, J., Lin, J., Gao, K., Yan, K., ming Yin, S., Bai, S., Xu, X., Chen, Y., Chen, Y., Tang, Z., Zhang, Z., Wang, Z., Yang, A., Yu, B., Cheng, C., Liu, D., Li, D., Zhang, H., Meng, H., Wei, H., Ni, J., Chen, K., Cao, K., Peng, L., Qu, L., Wu, M., Wang, P., Yu, S., Wen, T., Feng, W., Xu, X., Wang, Y., Zhang, Y., Zhu, Y., Wu, Y., Cai, Y., and Liu, Z. Qwen-image technical report, 2025a. URL <https://arxiv.org/abs/2508.02324>.

Wu, H., Xu, J., Le, H., and Samaras, D. Importance-based token merging for efficient image and video generation. In *Proceedings of the IEEE/CVF International Conference on Computer Vision*, pp. 4983–4995, 2025b.

Wu, J., Gan, W., Chen, Z., Wan, S., and Yu, P. S. Multimodal large language models: A survey. In *2023 IEEE International Conference on Big Data (BigData)*, pp. 2247–2256. IEEE, 2023.

Wu, J., Wang, H., Shang, Y., Shah, M., and Yan, Y. Ptq4dit: Post-training quantization for diffusion transformers. *Advances in neural information processing systems*, 37: 62732–62755, 2024.

Xing, Z., Feng, Q., Chen, H., Dai, Q., Hu, H., Xu, H., Wu, Z., and Jiang, Y.-G. A survey on video diffusion models. *ACM Computing Surveys*, 57(2):1–42, 2024.

Yang, S., Xi, H., Zhao, Y., Li, M., Zhang, J., Cai, H., Lin, Y., Li, X., Xu, C., Peng, K., et al. Sparse videogen2: Accelerate video generation with sparse attention via semantic-aware permutation. *arXiv preprint arXiv:2505.18875*, 2025.

Yu, Q., Chow, W., Yue, Z., Pan, K., Wu, Y., Wan, X., Li, J., Tang, S., Zhang, H., and Zhuang, Y. Anyedit: Mastering unified high-quality image editing for any idea. In *Proceedings of the Computer Vision and Pattern Recognition Conference*, pp. 26125–26135, 2025.

Zhai, X., Wang, X., Mustafa, B., Steiner, A., Keysers, D., Kolesnikov, A., and Beyer, L. Lit: Zero-shot transfer with locked-image text tuning. *CVPR*, 2022.

Zhang, J., Xiang, C., Huang, H., Wei, J., Xi, H., Zhu, J., and Chen, J. Spargettn: Accurate sparse attention accelerating any model inference. In *International Conference on Machine Learning (ICML)*, 2025a.

Zhang, P., Chen, Y., Huang, H., Lin, W., Liu, Z., Stoica, I., Xing, E., and Zhang, H. Vsa: Faster video diffusion with trainable sparse attention. *arXiv preprint arXiv:2505.13389*, 2025b.

Zhang, P., Chen, Y., Su, R., Ding, H., Stoica, I., Liu, Z., and Zhang, H. Fast video generation with sliding tile attention. *arXiv preprint arXiv:2502.04507*, 2025c.

Zhang, Q., Cheng, A., Lu, M., Zhuo, Z., Wang, M., Cao, J., Guo, S., She, Q., and Zhang, S. [cls] attention is all you need for training-free visual token pruning: Make vlm inference faster. *arXiv preprint arXiv:2412.01818*, 2024.

Zhang, Q., Cheng, A., Lu, M., Zhang, R., Zhuo, Z., Cao, J., Guo, S., She, Q., and Zhang, S. Beyond text-visual attention: Exploiting visual cues for effective token pruning in vlms. In *Proceedings of the IEEE/CVF International Conference on Computer Vision*, pp. 20857–20867, 2025d.

Zhang, R., Isola, P., Efros, A. A., Shechtman, E., and Wang, O. The unreasonable effectiveness of deep features as a perceptual metric. In *Proceedings of the IEEE conference on computer vision and pattern recognition*, pp. 586–595, 2018.

Zhang, Y., Fan, C.-K., Ma, J., Zheng, W., Huang, T., Cheng, K., Gudovskiy, D. A., Okuno, T., Nakata, Y., Keutzer, K., et al. Sparsevlm: Visual token sparsification for efficient vision-language model inference. In *Forty-second International Conference on Machine Learning*, 2025e.

Zhao, W., Han, Y., Tang, J., Wang, K., Song, Y., Huang, G., Wang, F., and You, Y. Dynamic diffusion transformer. *ICLR*, 2025.

Zou, C., Liu, X., Liu, T., Huang, S., and Zhang, L. Accelerating diffusion transformers with token-wise feature caching. *arXiv preprint arXiv:2410.05317*, 2024.

Zou, X., Lu, D., Wang, Y., Yan, Y., Lyu, Y., Zheng, X., Zhang, L., and Hu, X. Don’t just chase “highlighted tokens” in mllms: Revisiting visual holistic context retention. In *The Thirty-ninth Annual Conference on Neural Information Processing Systems*, 2025.

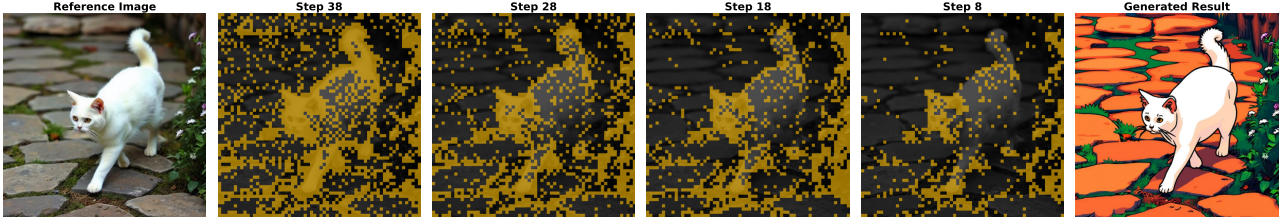


Figure 7. **Visualization of token selection dynamics across the diffusion trajectory.** We examine pruning outcomes at four distinct denoising stages: Early ($t = 38$), Middle ($t = 28, 18$), and Late ($t = 8$). The gold binary mask overlaid on the reference image represents the top- τ ($\tau = 0.85$) cumulative probability mass, highlighting the retained semantic anchors versus the pruned background.

A. Visualization of Token Selection Dynamics

This section empirically validates the precision of the ToPi mechanism and underscores the necessity of our periodic update strategy. Fig. 7 visualizes the evolution of the active token set throughout the denoising process. The visualization reveals a progressive sparsification of the active token set. As the denoising trajectory resolves latent structure, the model’s reliance shifts from external reference guidance to internal self-refinement. In the early stages, the generation necessitates broad semantic coverage from the reference to establish global structure. However, as the image takes shape, the generative process becomes increasingly driven by self-attention within the noisy tokens, reducing the need for extensive contextual support. Consequently, the cross-attention mechanism naturally discards the majority of reference tokens, retaining only sparse semantic anchors.

Algorithm 1 Inference with ToPi

```

1: Input: Prompt  $y$ , Noisy tokens  $\mathcal{G}^t$ , Reference tokens  $\mathcal{C}$ , RoPE  $\mathcal{P}$ ,  

   Update Timesteps  $\mathcal{T}_{\text{anchor}}$ , Representative Layers  $\mathcal{L}$ , Ratio  $\tau$ 
2: Output: Generated Image  $I_{\text{gen}}$ 
3: // Initialize: Start with full token retention
4:  $M \leftarrow 1$ 
5: for  $t = T$  to 1 do
6:   // 1. Common Front-End (Full Context)
7:    $\mathbf{H}_G, \mathbf{H}_C, \mathbf{H}_y \leftarrow \text{DiT}_{\text{front}}(\mathcal{G}^t, \mathcal{C}, y, \mathcal{P})$ 
8:   if  $t \in \mathcal{T}_{\text{anchor}}$  then
9:     // — Mode A: Full Inference & Mask Update —
10:    // Run with full reference to capture attention maps
11:     $\epsilon_{\theta}, \mathbf{A}_{\mathcal{L}}, \mathbf{V}_{\mathcal{L}} \leftarrow \text{DiT}_{\text{back}}(\mathbf{H}_G, \mathbf{H}_C, \mathbf{H}_y, \mathcal{P}, \text{return\_attn} = \text{True}, \text{anchor\_layers} = \mathcal{L})$ 
12:    // Update mask for future steps
13:     $\mathcal{I} \leftarrow \text{Aggregate}(\mathbf{A}_{\mathcal{L}}, \mathbf{V}_{\mathcal{L}})$ 
14:     $\mathcal{I}_{\pi}, \text{Indices} \leftarrow \text{SortDescending}(\mathcal{I})$ 
15:     $K \leftarrow \arg \min_k (\sum_{j=1}^k \mathcal{I}_{\pi}[j] \geq \tau \cdot I_{\text{total}})$ 
16:     $M \leftarrow \text{CreateMask}(\text{Indices}[0 : K])$ 
17:   else
18:     // — Mode B: Accelerated Inference —
19:     // Physically remove uninformative tokens (Hard Pruning)
20:      $\hat{\mathbf{H}}_C \leftarrow \mathbf{H}_C[M]$ 
21:      $\hat{\mathcal{P}} \leftarrow \text{cat}(\mathcal{P}[\mathcal{G}], \mathcal{P}[M])$ 
22:     // Run backend with reduced sequence length
23:      $\epsilon_{\theta} \leftarrow \text{DiT}_{\text{back}}(\mathbf{H}_G, \hat{\mathbf{H}}_C, \mathbf{H}_y, \hat{\mathcal{P}}, \text{return\_attn} = \text{False})$ 
24:   end if
25:   // 2. Standard Diffusion Step
26:    $\mathcal{G}_{t-1} \leftarrow \text{Step}(\mathcal{G}^t, \epsilon_{\theta})$ 
27: end for
28:  $I_{\text{gen}} \leftarrow \text{Decode}(\mathcal{G}_0)$ 

```

B. Detailed Algorithmic Formulation of ToPi

Algorithm 1 delineates the inference procedure of ToPi. To facilitate token-wise optimization, we conceptually partition the diffusion backbone (DiT) into a frontend (DiT_{front}) and a backend (DiT_{back}). Specifically, DiT_{front} comprises the first K layers, while DiT_{back} encompasses the remaining layers. The inference trajectory alternates between two distinct operational modes, governed by the update timesteps $\mathcal{T}_{\text{anchor}}$:

- **Mask Update Step** ($t \in \mathcal{T}_{\text{anchor}}$): During these denoising steps, the model executes a full-reference inference pass via DiT_{back} to extract precise inter-token cross-attention maps \mathbf{A} . These maps are aggregated to quantify token saliency, which subsequently recalibrates the binary selection mask M for future iterations.
- **Accelerated Step** ($t \notin \mathcal{T}_{\text{anchor}}$): During these denoising steps, the pre-computed mask M is applied to physically prune redundant reference tokens (Hard Pruning). This yields a compressed latent representation \hat{H}_C , allowing DiT_{back} to operate on a significantly reduced sequence length, thereby minimizing computational overhead without compromising semantic fidelity.

C. Implementation Details

C.1. Model Architecture

- **Flux.1-Kontext** (Labs et al., 2025). Flux.1-Kontext is a 12B parameter rectified flow transformer specialized for text-instruction-based image editing. Based on the FluxTransformer2DModel architecture, it incorporates explicit guidance embeddings and features a hybrid layer structure consisting of 19 dual-stream attention layers and 38 single-stream layers.
- **Qwen-Image-Edit** (Wu et al., 2025a). Qwen-Image-Edit is an image editing model built upon the 20B parameter Qwen-Image foundation, designed to integrate text rendering capabilities with precise semantic and appearance control via Qwen2.5-VL and a VAE encoder. Architecturally, it utilizes the QwenImageTransformer2DModel structure, featuring a deep configuration of 60 transformer layers.

C.2. Hardware Environment

All evaluations were conducted on:

- **Flux.1-Kontext:** NVIDIA A100 (40GB) GPU.
- **Qwen-Image-Edit:** NVIDIA H20 (96GB) GPU.
- **Software:** PyTorch 2.4 with FlashAttention enabled for memory efficient attention.

C.3. Calibration

To ensure the robustness and generality of the identified Representative Layers (\mathcal{L}), we constructed a diverse calibration set of 48 image-text pairs. Crucially, these samples were stratified across varying subtasks (e.g., Local Editing, Global Editing) to avoid task-specific bias. We observed that the distribution of layer sensitivity remained consistent across these subtasks, supporting our hypothesis that layer importance is structurally intrinsic. Meanwhile, calibration is a one-time offline procedure per architecture, incurring zero runtime overhead during inference. Specifically, we identified $\mathcal{L} = \{13, 18, 31\}$ for Flux.1-Kontext and $\mathcal{L} = \{35, 37, 42\}$ for Qwen-Image-Edit.

D. More Qualitative Results

To further evaluate the robustness and generalization ability of ToPi, we provide extended qualitative comparisons across a broader range of editing scenarios.

D.1. Single Image

Due to space constraints in the main text, we present additional qualitative comparisons here. Fig. 8 demonstrates the performance of ToPi across a wider variety of tasks, including complex scene composition and style transfer. As observed,



Figure 8. Qualitative comparison against ToMeSD and ToMA on the AnyEdit benchmark. The visualization is bilaterally partitioned: the left panel utilizes the **Flux.1-Kontext** backbone, while the right panel employs **Qwen-Image-Edit**. Best viewed zoomed in.

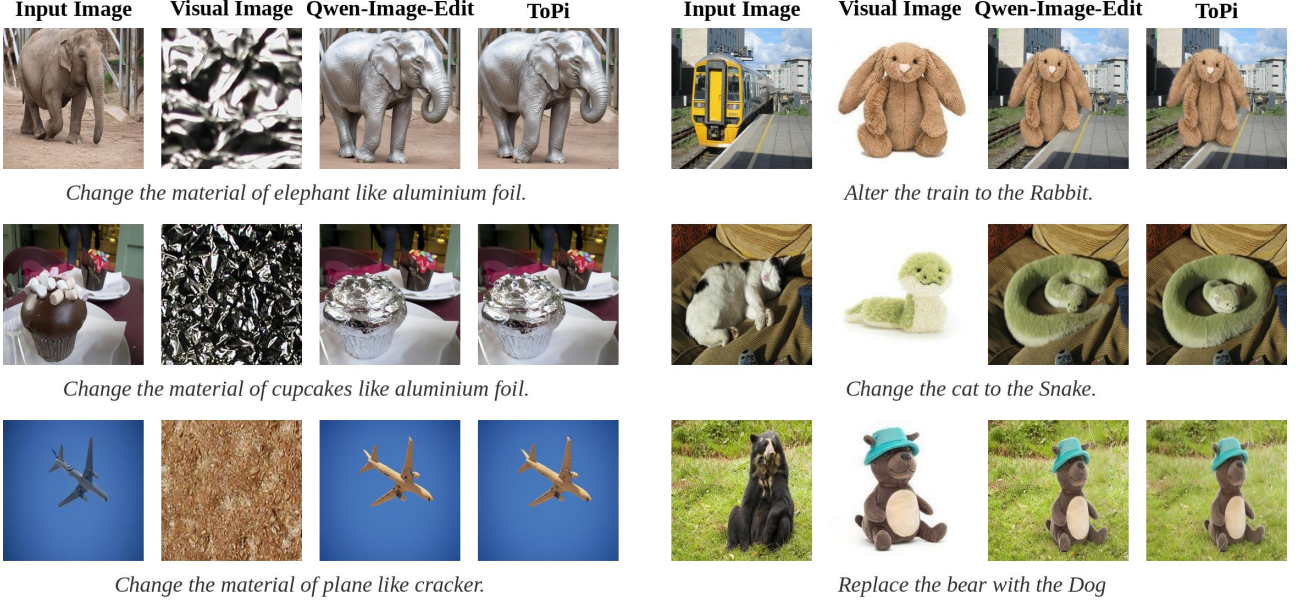


Figure 9. Qualitative comparison on multi-image reference editing tasks.

our method maintains high fidelity to the reference subject, whereas baseline methods often lose fine-grained details or exhibit artifacts in texture generation.

D.2. Multiple Image

We extend our evaluation to multi-image scenarios using the Qwen-Image-Edit architecture. Fig. 9 compares our pruned model (ToPi) against the full-context inference baseline across tasks like visual material transfer and reference-guided object replacement. As observed, ToPi maintains high generation fidelity despite the token pruning. It successfully preserves structural integrity during texture mapping and maintains object identity during reference-guided replacement. These results confirm that our metric accurately identifies and retains the critical semantic tokens required for complex, multi-input generation, achieving performance parity with the full-context baseline.

E. More Ablation Results

E.1. Impact of Pruning Threshold τ

We investigate the sensitivity of ToPi to the pruning threshold τ . Fig. 10 provides a qualitative visualization of the generated samples across varying τ values. As observed, our method maintains high visual fidelity and structural consistency even under aggressive pruning rates (e.g., $\tau = 0.8$). The results demonstrate that ToPi effectively removes redundant tokens without compromising the semantic integrity of the generated images.

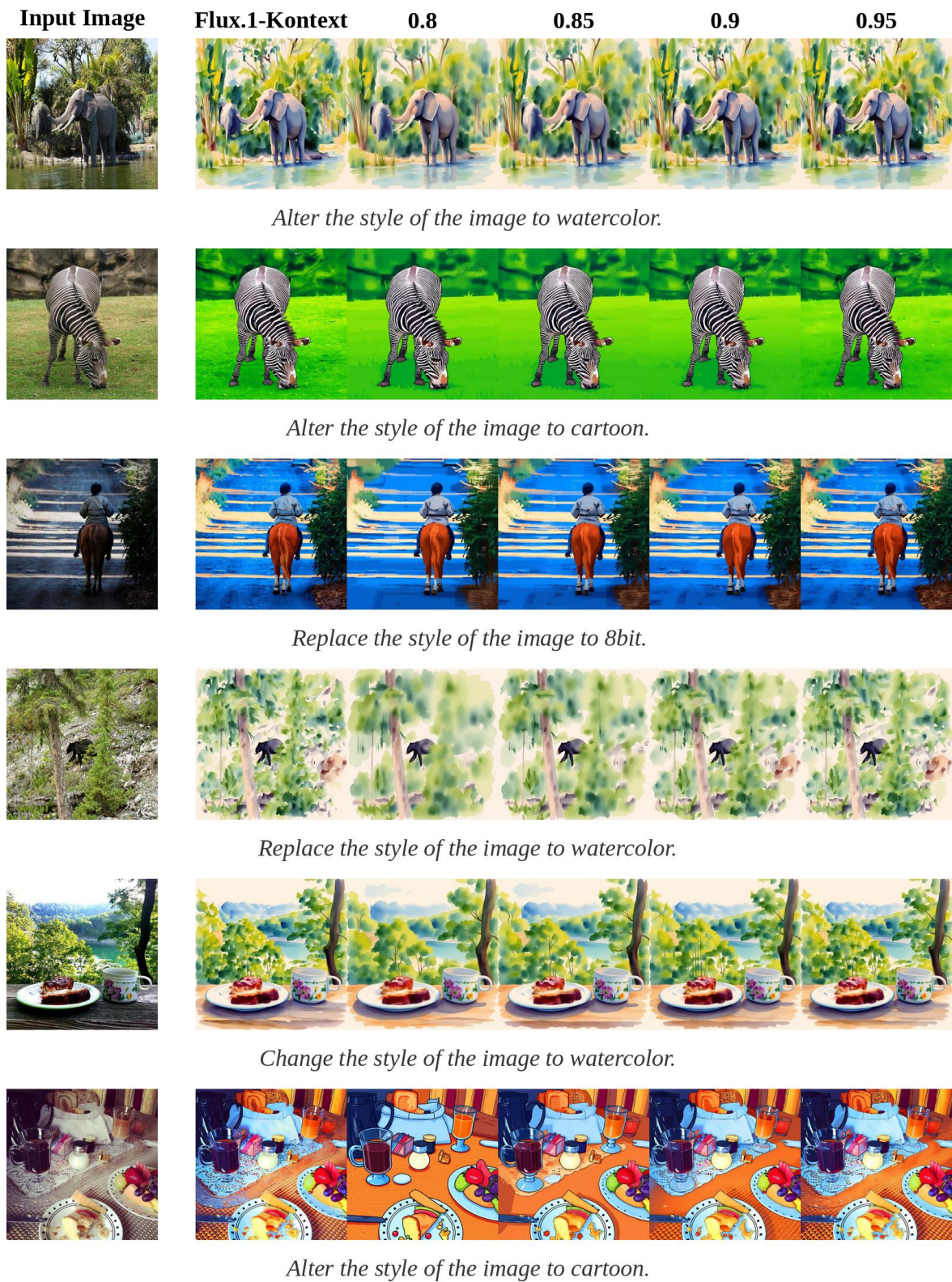


Figure 10. Qualitative visualization of the generated samples across varying τ values.

E.2. Prune vs Merge

Table 4. Quantitative comparison across different editing categories. The best results are highlighted in **bold**.

Category	PSNR \uparrow		SSIM \uparrow		LPIPS \downarrow	
	Prune	Merge	Prune	Merge	Prune	Merge
Camera Move	27.69	26.12	0.828	0.799	0.108	0.136
Global Edit	23.76	21.84	0.754	0.708	0.173	0.224
Implicit Change	30.02	28.27	0.874	0.850	0.088	0.119
Local Edit	27.52	25.75	0.862	0.830	0.091	0.121

Tab. 4 provides a quantitative ablation study comparing two distinct token reduction strategies within our DiT framework: *Prune* (selective retention) and *Merge* (token aggregation). To ensure a fair comparison, the *Merge* baseline utilizes the same Token Influence Score (I_j) for ranking. However, instead of discarding the less important tokens, we aggregate them into their nearest retained neighbors via feature averaging. The results indicate that the merging strategy consistently lags behind the pruning approach across all editing categories. We hypothesize that merging tokens inevitably introduces feature over-smoothing, where distinct high-frequency details are averaged out, leading to higher LPIPS values (0.224 vs. 0.173 in Global Editing). Conversely, *Prune* preserves the original feature integrity of the most critical tokens, thereby achieving superior fidelity.

E.3. Comparison with Static Layer Selection.

Table 5. Quantitative comparison of layer selection strategies. We benchmark our adaptive method against static heuristics (*First*, *Last*) and aggregation baselines (*Random*, *All*).

Category	Selection Strategy	PSNR \uparrow	SSIM \uparrow	LPIPS \downarrow
Camera Move	First	27.10	0.817	0.118
	Last	24.31	0.772	0.149
	Random	26.80	0.819	0.112
	All	27.43	0.822	0.113
	Ours	27.69	0.828	0.108
Global Editing	First	22.76	0.731	0.195
	Last	22.13	0.726	0.198
	Random	23.13	0.740	0.184
	All	23.64	0.751	0.176
	Ours	23.76	0.754	0.173
Implicit Change	First	29.35	0.866	0.097
	Last	27.55	0.857	0.107
	Random	29.31	0.868	0.090
	All	30.00	0.870	0.091
	Ours	30.02	0.874	0.088
Local Editing	First	26.93	0.845	0.104
	Last	25.21	0.832	0.119
	Random	26.62	0.849	0.099
	All	27.48	0.854	0.097
	Ours	27.52	0.862	0.091

Complementing the discussion on *Random* and *All* strategies in the main text, here we further benchmark our method against two deterministic heuristics: (1) *First*, which selects the initial 3 layers; and (2) *Last*, targeting the final 3 layers. As detailed in Tab. 5, two key observations support the necessity of our adaptive selection mechanism. **First, static heuristics are insufficient.** The *Last* strategy yields the lowest performance across all categories (e.g., PSNR 24.31 vs. 27.69 in Camera Move), suggesting that the deepest layers in DiT may focus more on high-frequency noise prediction rather than semantic context alignment. While *First* performs better, it still lags behind *Ours*, indicating that critical information is not strictly confined to the shallowest layers. **Second, representative layer anchoring is crucial.** Unlike these fixed strategies, our method dynamically isolates layers with high context sensitivity scores $S^{(\ell)}$. This effectively filters out non-informative layers (avoiding the noise introduction seen in *All*) while capturing essential semantic features that static strategies miss.

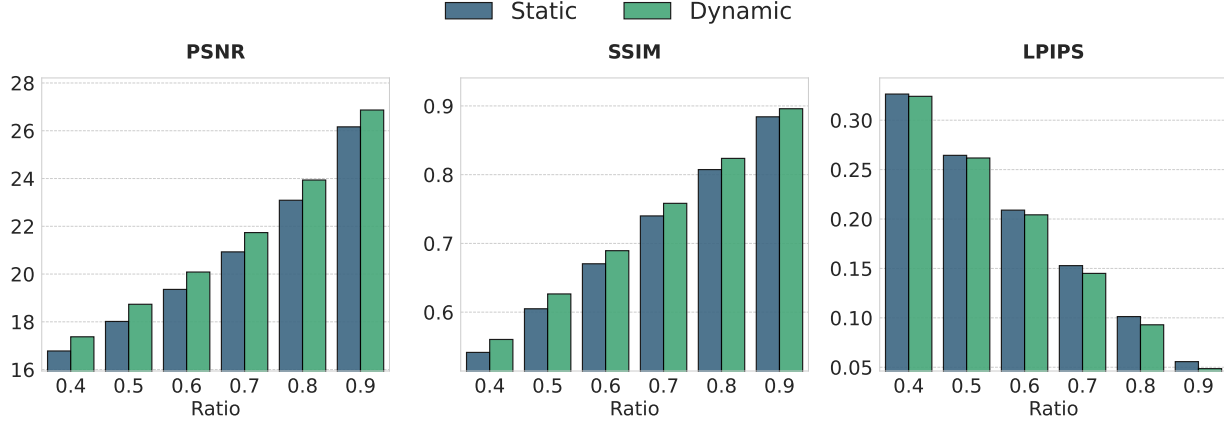


Figure 11. Effectiveness of Temporal Adaptation

E.4. Impact of Temporal Adaptation

We validate the necessity of the token mask update (Eq. 11) by comparing ToPi against a *Static* baseline where the context set is determined once at initialization. As shown in Fig. 11, our dynamic strategy consistently outperforms the static approach across all metrics (PSNR, SSIM, LPIPS). This confirms that a fixed token subset fails to accommodate the evolving semantic focus of the diffusion process (e.g., from structure to texture), whereas our temporal adaptation effectively captures these critical shifts.

F. Detailed Complexity and FLOPs Analysis

We provide a comprehensive theoretical analysis of the computational complexity and a breakdown of the FLOPs reduction achieved by ToPi.

F.1. Theoretical Complexity Analysis: Joint vs. Single Blocks

Based on the official implementation of Flux.1-Kontext and Qwen-Image-Edit, we derive the computational complexity for its two distinct block types: Double Stream Block and Single Stream Block. Based on the `QwenDoubleStreamAttnProcessor` implementation, Qwen-Image-Edit employs a transformer block mechanism similar to the Flux Double Stream Block, operating at a large scale (e.g., hidden dimension $d = 4096$ and substantial layer number $L = 60$). Let N_{img} be the number of visual tokens, N_{prompt} the number of prompt text tokens, and d the hidden dimension.

1. Double Stream Block. This block processes streams independently for linear projections but jointly for attention.

- **Joint Attention:**

$$\mathcal{C}_{JointAttn} \approx \underbrace{4(N_{img} + N_{prompt})^2 d}_{\text{Attention Core}} \quad (13)$$

- **Dual FFNs:**

- Flux.1-Kontext: Separate MLPs ($d \rightarrow 4d \rightarrow d$) are applied to each stream.

$$\mathcal{C}_{DualFFN} \approx \underbrace{16N_{img}d^2}_{\text{Image FFN}} + \underbrace{16N_{prompt}d^2}_{\text{Text FFN}} + \underbrace{8(N_{img} + N_{prompt})d^2}_{\text{Q,K,V,O Projections}} = 24(N_{img} + N_{prompt})d^2 \quad (14)$$

- Qwen-Image-Edit: Separate MLPs ($d \rightarrow 6d \rightarrow d$) are applied to each stream.

$$\mathcal{C}_{DualFFN} \approx \underbrace{24N_{img}d^2}_{\text{Image FFN}} + \underbrace{24N_{prompt}d^2}_{\text{Text FFN}} + \underbrace{8(N_{img} + N_{prompt})d^2}_{\text{Q,K,V,O Projections}} = 32(N_{img} + N_{prompt})d^2 \quad (15)$$

Note: Standard Gated MLP adds slight overhead, approximated here as standard $d \rightarrow xd \rightarrow d$ cost.

Table 6. Single-Layer FLOPs Breakdown (GFLOPs). Comparison under heavy context load ($N_{total} \approx 8.7k \rightarrow 6.6k$). ToPi effectively reduces the quadratic attention bottleneck and the massive linear operations associated with the visual stream.

Architecture	Component	Baseline (GFLOPs)	ToPi (GFLOPs)	Reduction (%)	Mechanism
Flux Joint <i>(Double Stream)</i> $d = 4096$	Joint Attn Core (N_{tot}^2)	1241.25	725.85	-41.5%	Quadratic Linear Fixed Overhead
	Image Linear Ops (N_{img})	3298.53	2473.90	-25.0%	
	Text Linear Ops (N_{prompt})	206.16	206.16	0.0%	
	Layer Total	4745.94	3405.91	-28.2%	
Flux Single <i>(Single Stream)</i> $d = 4096$	Single Attn Core (N_{tot}^2)	1241.25	725.85	-41.5%	Quadratic Linear (Fused)
	Single Linear Ops (N_{tot})	3504.69	2680.06	-23.5%	
	Layer Total	4745.94	3405.91	-28.2%	
	Layer Total	5914.17	4299.26	-27.3%	

2. Single Stream Block. This block concatenates inputs ($N_{total} = N_{img} + N_{prompt}$) and employs a parallel Attention-MLP architecture with a fused output.

- **Single Attention Core:**

$$\mathcal{C}_{SingleAttn} \approx 4(N_{img} + N_{prompt})^2 d \quad (16)$$

- **Single Linear Operations:** The block computes Q,K,V ($3d^2$), an MLP up-projection ($4d^2$), and a large fused output projection that maps the concatenated Attention+MLP output ($d + 4d$) back to d ($5d^2$).

$$\mathcal{C}_{SingleLinear} \approx \underbrace{(6 + 8 + 10)N_{total}d^2}_{QKV + MLP_Up + Fused_Out} = 24(N_{img} + N_{prompt})d^2 \quad (17)$$

Eventually, we can see that the theoretical complexity is the same for both categories.

F.2. ToPi Complexity.

ToPi Complexity. ToPi prunes the reference tokens in the visual stream ($N_{img} \rightarrow \hat{N}_{img}$). This provides a quadratic reduction in the Attention mechanism ($\hat{N}_{img} + N_{prompt}$) 2 and a linear reduction in the Visual FFN. The Text FFN cost remains constant but is negligible compared to the visual computation.

Overhead Analysis. The additional cost introduced by ToPi involves the Importance Scoring and Selection phases.

- **Scoring:** The computation of Token Influence Score I_j requires aggregating attention maps from a subset of representative layers $|\mathcal{L}|$. This incurs $O(|\mathcal{L}| \cdot |\mathcal{G}| \cdot |\mathcal{C}|)$. However, since this is only performed at sparse update intervals ΔT (e.g., every 10 steps), the amortized cost is negligible: $\frac{1}{\Delta T} \cdot O(|\mathcal{L}| \cdot |\mathcal{G}| \cdot |\mathcal{C}|) \approx 0$.
- **Selection:** The sorting and gathering operation has a complexity of $O(|\mathcal{C}| \log |\mathcal{C}|)$, which is computationally trivial compared to the matrix multiplications in attention layers.

F.3. Single-Layer FLOPs Breakdown

We provide a granular breakdown of the FLOPs for a single transformer layer. We analyze a heavy in-context generation scenario where the visual input consists of noisy tokens ($|\mathcal{G}| = 4096$) and dense reference tokens ($|\mathcal{C}| = 4096$), totaling $N_{img} = 8192$ visual tokens. The condition (text or multimodal prompts) is $N_{prompt} = 512$.

ToPi prunes the reference tokens by 50% ($4096 \rightarrow 2048$), reducing the total visual tokens to $N'_{img} = 6144$.

Observation. As shown on Tab. 6, in this high-load regime ($N \approx 8k$), the **Joint Attention Core** consumes a significant portion of compute ($\approx 30\%$ of total FLOPs).

Table 7. Runtime breakdown analysis of Flux.1-Kontext. The data represents a typical inference session with 1024×1024 resolution and 40 sampling steps. With a pruning threshold of 0.85 and an update interval of $\Delta T = 10$, the proposed modules add less than 1% overhead.

Component	Runtime (s)	Ratio (%)
Base Model Inference	27.692	99.45%
Importance Scoring	0.147	0.50%
Selection	0.014	0.05%
Total	27.853	100.0%

F.4. Overhead Breakdown

Overhead Analysis. The additional computational cost introduced by ToPi stems primarily from two phases: *Importance Scoring* and *Selection*. We analyze the overhead from both theoretical complexity and empirical runtime perspectives. To quantify the actual latency of Flux.1-Kontext, we present a representative case in Tab. 7. The evaluation is conducted under the following configuration: image resolution of 1024×1024 for both generation and reference, a pruning threshold of 0.85, an update interval $\Delta T = 10$, and a total of 40 inference steps. Under these settings, the *Importance Scoring* consumes only 0.147s (0.50% of total runtime), and the *Selection* takes a negligible 0.014s (0.05%). This confirms that ToPi introduces virtually no perceptible latency to the standard inference pipeline.